We are IntechOpen,
the world's leading publisher of
Open Access books
Built by scientists, for scientists

4,800
Open access books available

122,000
International authors and editors

135M
Downloads

Our authors are among the

154
Countries delivered to

TOP 1%
most cited scientists

12.2%
Contributors from top 500 universities

CLARIVATE ANALYTICS
BOOK CITATION INDEX
INDEXED

WEB OF SCIENCE™

Selection of our books indexed in the Book Citation Index
in Web of Science™ Core Collection (BKCI)

Interested in publishing with us?
Contact book.department@intechopen.com

Numbers displayed above are based on latest data collected.
For more information visit www.intechopen.com

Efficient Microbial Decontamination of Translucent Liquids and Gases Using Optical Metamaterials

Nicolae Enaki, Sergiu Bizgan, Andrei Nistreanu,
Viorica Tonu, Marina Turcan, Tatiana Pislari,
Elena Starodub, Aurelia Profir,
Gianina-Florentina Popescu-Pelin, Maria Badiceanu,
Carmen-Georgeta Ristoscu and Ion N. Mihailescu

Abstract

An effective way of decontamination using optical metamaterials like photonic crystals consisting of glass microspheres or granulated quartz with various geometries is proposed. The efficient decontamination using the evanescent zone of metamaterials opens a new perspective in pathogen decontamination. We propose different topological structures of metamaterials to enlarge the contact surface of ultraviolet radiation with polluted translucent fluids. The approach is based upon the increased transfer of UV radiation via evanescent waves of metamaterials into contaminated translucent fluids. A series of experimental estimations of the decontamination rate of this type of metamaterials have been made. For these investigations, a decontamination core filled up with metamaterials is used through which the contaminated fluid freely flows. Experiments have conclusively proved that evanescent zone of quartz and optical fiber metamaterials can effectively inactivate *Coliform* (including *Escherichia coli*), or *Enterococcus* bacteria, as well as yeast and *Kombucha* cultures.

Keywords: metamaterials, evanescent zone, Raman excitation, decontamination, pathogen

1. Introduction

Recently, the peculiarities of metamaterials and nanoparticles are used in the construction of new devices for optoelectronics [1]. The research on photonic terahertz and microwave electromagnetic devices by using the nonlinear properties of metamaterials has been summarized. The periodicity of the building blocks of metamaterials which are smaller than the light wavelength was taken into consideration. The nanoparticle devices can be used for the localization of cavity fields, in particular surface plasmon resonance (SPR) [2]. Some of the phenomena originated by the uncommon wave dynamics in near-zero photonics and their fundamental and technological implications on different subfields of optics and metamaterials are presented in Ref. [3].

One concern in pathogen decontamination is the need of a new effective method of radiation interaction with microorganisms [4–6]. An open surface of a translucent fluid exposed to radiation cannot provide the expected solution, due to the difficulty to irradiate pathogens inside the liquid volume as an immanent self-absorption. In this case, the total contact surface in quasi-periodical structures comes to be proportional to the surface of one element multiplied by the number of elements. Accordingly, the decontamination volume increases due to the large dispersion of light in these metamaterials, being proportional to the surface of one element multiplied to their number and UV-C light penetration depth through the translucent contaminated fluid.

The use of optical metamaterials with periodical structures to act against *undesired microorganisms* (viruses, bacteria, and yeast) existing in translucent liquids and gases is proposed. Studies were devoted to the topological effect of individual metamaterial elements on the modification of UV (ultraviolet) absorption of evanescent waves dispersed in the optical contact zones, as a function of granule size and geometry. The decontamination rate also depends on the packing and optical properties of metamaterial elements, as well as on the optical properties of contaminated liquids and microorganisms inside them. Different situations were investigated, when quartz (SiO_2) or glass metamaterials with dimensions of about 0.5–3 mm are separately placed into a quartz core tube, of about 2.7 cm diameter and 90 cm length, of decontamination equipment. Quartz granules transmit UV light (240–400 nm) of the Hg lamp and ensure an efficient microbial decontamination of translucent liquids and gases. We herewith demonstrate the efficient antimicrobial action of the evanescent waves dispersed around quartz metamaterial elements inside contaminated translucent fluids.

The decontamination rate was studied in different configurations of metamaterials such as microspheres and unordered granules, with the aim to obtain an efficient contact zone of the contaminated liquids with UV radiation. This effect can be boosted by the manipulation of microorganisms along the optical fibers or around microspheres. A special trapping zone could be identified by exploration of high-density viruses and bacteria interaction with metamaterials in order to annihilate pathogens.

We herewith propose a model for structures with optical periodicity characterized by large free spaces among elements and fitting evanescent zone. This proves essential for decontamination of fluids that flow close to surface of microspheres or optical fibers. Here, one should asses the adherence of liquids to surface, evanescent field penetration depth inside contaminated fluid, and coefficient of absorption of light radiation by microorganisms.

We analyzed the contact surfaces between the contaminated fluid and optical metamaterials, like photonic crystals or unordered granules, inserted inside the "core tube" of the decontamination reactor. In this case, the dispersive optical systems connected with the liquid volume through evanescent field improve the contact zones between UV radiation and pathogens. The dynamic treatment regime of translucent liquids that flow through decontamination core tube filled up with metamaterials is discussed. Moreover, the static treatment regime is analyzed, in which the fluids filling up the free spaces between metamaterial's elements keep motionless. When increasing the dimension of metamaterial elements, the decontamination rate decreases due to the increasing of distance between elements and the weaker penetration of the radiation into the liquid.

One expects a large increase of the observed effects when passing from simple lamps to laser irradiation, that is, incoherent to coherent light sources. Also, significant improvement is expected when using optical fibers for evanescent wave generation instead of, or in parallel with, quartz microspheres. Our results prove that the energy emerging via evanescent waves from multistructures under dynamic irradiation is not in any case lost but used in this particular case for the efficient antimicrobial action. This can contribute to a positive balance of light propagation through optical metamaterials and fiber metamaterials in view of valorizing all resources with maximum efficiency.

The approach presented in this chapter proposes a new method of decontamination using metamaterials consisting of microspheres and optical fibers structures with various topologies. The proposed method secures a substantial gain in the decontamination contact surfaces between the contaminated fluid and metamaterials, inserted inside the "core tube" of the decontamination reactor during the light (UV) propagation. The efficient decontamination using the evanescent zones of metamaterials opens new perspectives, not simply for new and innovative research applications, but besides opens novel ways for fundamental studies. The cumulative effect of UV radiation in contact with contaminated liquid depends on the refractive index of metamaterial and liquid, as well as optical properties of pathogens. A decontamination complementary effect depends on the probable trapping of liquid microparticles into the evanescent zone of optical fibers or microspheres in photon crystal structures [7, 8]. In this case, throughout the wave's propagation in nanofibers, a predilection for trapping and manipulating microparticles (viruses and bacteria) along the optical fibers occurs. The trapping of dielectric particles along the fibers was observed and revealed a new perspective on the capabilities of trapping the viruses, bacteria, and other microorganisms which can be present in contaminated liquids. Several techniques are proposed in order to destroy undesirable viral or bacterial particles [9]. These methods mainly used the UV lamp radiation for sterilization, but, quite often, they induced damaging effects and issues connected with the penetration depth. For instance, the 253 nm radiation effectively disinfects the surface, but sometimes, this emission could harm not just the viral particles and bacteria, but also mammalian cells [10–14]. When the intensity of UV irradiation is increased, the decontamination is always associated with mutation and shadowing effects, or damage of the viral nucleic acids and protein shells [11–14]. In other cases, radiation of microwave origin is proposed, but the absorption is not considered efficient because the energy is mostly transferred to water and not to the viral particles [12].

These drawbacks can be overcome by solving-related problems. The first one is associated with the UV radiation penetration depth. To solve this, it is required to propose an optical

system, which allows reaching large penetration of the radiation inside contaminated liquids (or gases). Second, it is needed to use the method of selective short pulse decontamination [9, 12, 13] for the estimation of the potential penetration depth in translucent liquids. For example, in Refs. [12, 13], the authors proposed a photonic approach for selective neutralization of viruses. In Ref. [12], a near-infrared (IR) ultrashort pulsed (USP) subpicoseconds fiber laser source is used instead of UV lamps to avoid IR absorption. This UPS targets only the weak links on the protein shells of viral particles. By selecting the appropriate laser parameters, the authors reveal that it is possible to damage the protein shells, conducting to their inactivation, but without affecting mammalian cells. More exactly, they demonstrated that this method can discriminate and inactivate viral particles, from nonpathogenic viruses such as M13 bacteriophage and tobacco mosaic virus (TMV) to pathogenic ones like human papillomavirus (HPV) and human immunodeficiency virus (HIV). Concomitantly, the sensitive materials, for example, human Jurkat T cells, human red blood cells, and mouse dendritic cells, keep unaffected. In Ref. [13], a mechanical model is proposed. It has a normal mode where it oscillates around its equilibrium geometry. By selecting the visible or near-IR laser pulse duration to be shorter or near to the normal oscillation period, the authors of Ref. [12] have demonstrated that a single beam excitation laser pulse can bring a macroparticle, as for example, a virus, into oscillation by impulsive stimulated Raman [14]. It is worthy to mention that similar coherent Raman effect for larger frequencies of UV pulses is used for diagnostics of the various biomolecules (e.g., lipids) with optical equipment [15, 16].

2. Nonlinear models of molecule interaction with short-pulse radiation

UV-C radiation is effective for inactivating protozoa, bacteria, viruses, and many microorganisms. According to literature [17–21], the use of UV-C radiation is especially a good, environment-friendly, and chemical-free method to inactivate dangerous pathogens in diverse condition. UV-C cannot pass through our atmosphere, so it does not contribute to DNA damage. However, it is worth to mention that UV-C lamps give effective results in killing bacteria and microbes.

The process of decontamination by UV radiation, which can cause thymine dimers of bacteria and viruses, is not yet fully understood [17]. Bactericidal mechanism of UV-C has a maximal damage to RNA and DNA. This process is accompanied by generation of pyrimidine residues in the nucleic acid strands. The consequence of this modification is a production of cyclobutane pyrimidine dimers that induces deformation of the DNA molecule. This might cause local vibration energy of the modes that may be coupled by nonharmonic, nonlinear term. For example, two vibration defects in cell replication can lead to cell death eventually (**Figure 1**).

Ref. [22] demonstrated that when exposing *E. coli* DNA to UV-C irradiation, randomly placed, dose-dependent, single-strand breaks are generated. It was proposed that the negative supercoiling strain on the DNA backbone is generated by the conformational relaxation. It has been often proved that as a result of the inactivation of bacteria and DNA viruses under UV action, thymine dimers are produced. A dose of 4.5 J/m^2 is testified to cause 50,000 pyrimidine dimers per cell [23]. It has been reported that 100 J/m^2 induces approximately
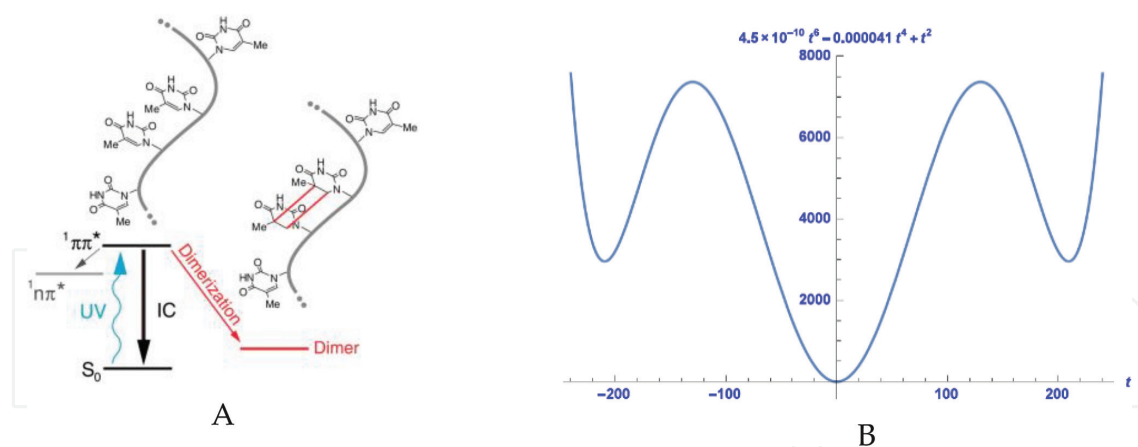
Figure 1. (A) Dimer bond generation under UV-C radiation of DNA according to Ref. [22] and (B) two-dimension potential with two minimums. First minimum corresponds to nondimer DNA and second minimum is similar to the dimer phototransformation of DNA under the UV-C radiation.

seven pyrimidine dimers per viral genome in SV40, which is sufficient to strongly inhibit viral DNA synthesis [24]. Thymine dimers formed within short pulse of UV excitation are properly oriented [19]. Only a few percent of the thymine doublets are expected to be favorably sited for reaction and dimerization at the moment of UV excitation.

a. **Figure 2(A)** explains the dimerization process for a thymine doublet having the appropriate orientation. The two most common conformations of DNA are A-DNA and B-DNA. Molecular orientations can fluctuate due to A and B conformations and vibrational or other movements of the DNA molecule. The average twist angle between consecutive base pairs varies with a few degrees only between the A and B conformations. The minor amount of conformational variation in A-DNA versus B-DNA explicates the superior resistance of A-DNA to cyclobutene pyrimidine dimer.

b. UV could induce cross-links between nonadjacent thymine besides cross-links between adjacent thymine, as illustrated in **Figure 2(B)**. Cross-linking than can be produced between the nucleotides and proteins in the viruses' capsid could damage the capsid of DNA viruses.

c. Cross-linking with cytosine and guanine requires higher energy because of three hydrogen bonds instead of two for thymine/adenine bonds. Accordingly, the thymine dimers are predominant. Thymine may also induce links with proteins, including the ones in the capsid (as is the case for viruses), as illustrated in **Figure 2(C)**. Other biological molecules with unsaturated bonds such as coenzymes, hormones, and electron carriers are prone to UV damage. In RNA (prokaryotic cells, eukaryotic cells, or viruses), uracil replaces thymine. The inactivation of RNA viruses is accompanied by cross-linking between the uracil nucleotides and the generation of uracil dimers [25]. These dimers could damage the capsid of RNA viruses, too. There exist limited quantitative data about the specific damage of DNA produced by UV absorption. Ref. [25] demonstrated that the UV exposure of mengovirus induces a fast formation of uracil dimers. This seemed to be the main source of virus inactivation. During 10 min of UV irradiation, a maximum of 9% of the total uracil dimers of the viral DNA are formed. Studies also demonstrated that irradiated viral RNA

converts into a viral protein covalently linked. Moreover, a slow destruction process of capsid occurred and photoproducts were produced. In the virus irradiated by UV appeared a covalent linkage of viral RNA to viral polypeptides, the most probably due to close vicinity of RNA and proteins in the capsid. The protein linked covalently to the RNA does not surpass 1.5% of the total protein capsid. The authors of Ref. [26] studied Venezuelan equine encephalitis (VEE) under UV irradiation and found evidence suggesting that the formation of uracil dimers led to extensive contacts of the RNA with protein in the nucleocapsid.

Taking into consideration the important advantages of vibrational spectroscopy based on nonlinear coherent anti-Stokes generation mechanism, the new technique *coherent anti-Stokes Raman spectroscopy (CARS)* was reported by authors of Ref. [27] as an attractive tool for rapid excitation of vibrational modes. The application of USP lasers in coherent Raman scattering (CRS) or CARS opens the new possibilities in the decontamination procedures of fluids by dangerous pathogens (viruses and bacteria). In many cases for the effective inactivation procedure of pathogens on the implant surface, it is necessary to take into consideration the relative dimensions of viruses and bacteria and their possible molecular vibration symmetry [28, 29]. Most natural viruses depend upon the existence of capsids with specific geometry, protective shells of various sizes composed of protein subunits (**Figure 3**). Up to now, the general shaping capsid design is still elusive. Therefore, the correct understanding of their properties may help to realistically block the virus life cycle and, consequently, design of efficient nanoassemblies.

The authors of Ref. [30] reveal an exceptional and species-independent evolutionary pressure on virus aphids. It is based on the concept that the simplest capsid designs are the best. This holds true for all existing virus capsids. As a consequence of theories, it results a substantially significant periodic table of virus capsids that reveals strong and predominant evolutionary pressures. It also offers geometric explanations for other capsid properties (rigidity, pleomorphic, auxiliary requirements, etc.), which earlier were considered to be unique for an individual virus.
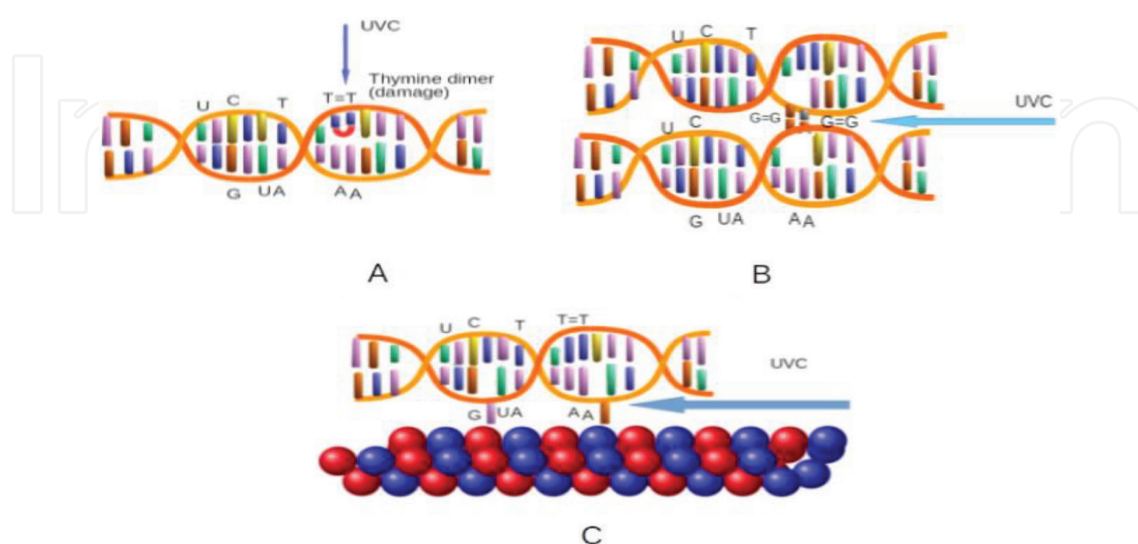

Figure 2. (A) Damage bonds and generation of dimer bonds under UV-C radiation of DNA. UV-C may also induce cross-links between nonadjacent thymine illustrated in (B). Cross-linking can occur with proteins, cytosine, and guanine (C).
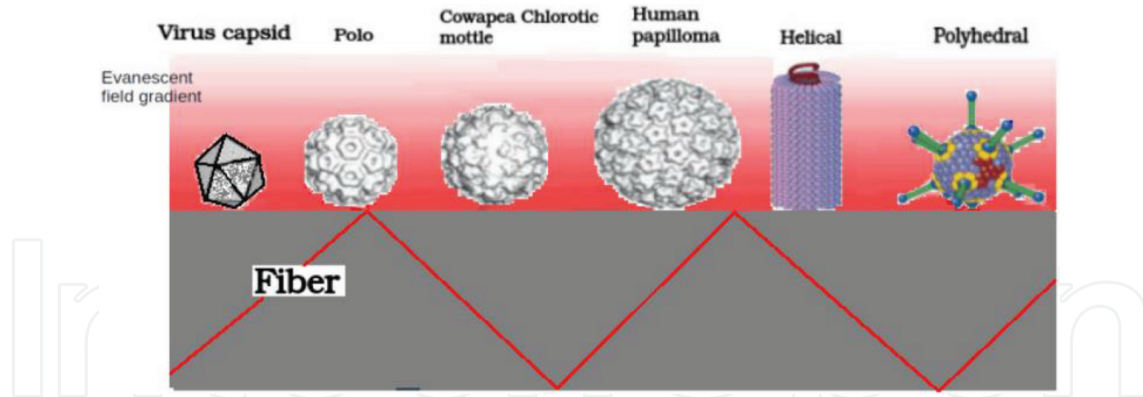
Figure 3. Relative dimension of viruses (bacteria) and their commensurability with the evanescent zone of a fiber optic. The spherical symmetry of the human papilloma, cowpea chlorotic mottle, and polo viruses. Some topological structures of polyhedral and helical viruses. Reproduced with permission from [6].

In our opinion, intrinsic topology of DNA dimmers (see **Figure 4**) may help to properly consider the symmetry vibration modes of this virus structure, such as to estimate the probable nonharmonic excitation of virus constituents by selectively annihilating them for the duration of the coherent Raman excitation. In the following, the method for exciting local vibration modes of biomolecule nanoassemblies is presented.

Most natural viruses depend upon the existence of spherical capsids: protective shells of various sizes composed of protein subunits (see **Figure 4**). Here, we must estimate the commensurability of virus dimensions with the depth of the evanescent zone of radiation around the metamaterials. So far, general evolutionary pressures shaping capsid design have remained elusive, even though an understanding of such properties may help in rationally impeding the virus life cycle and designing efficient nanoassemblies.
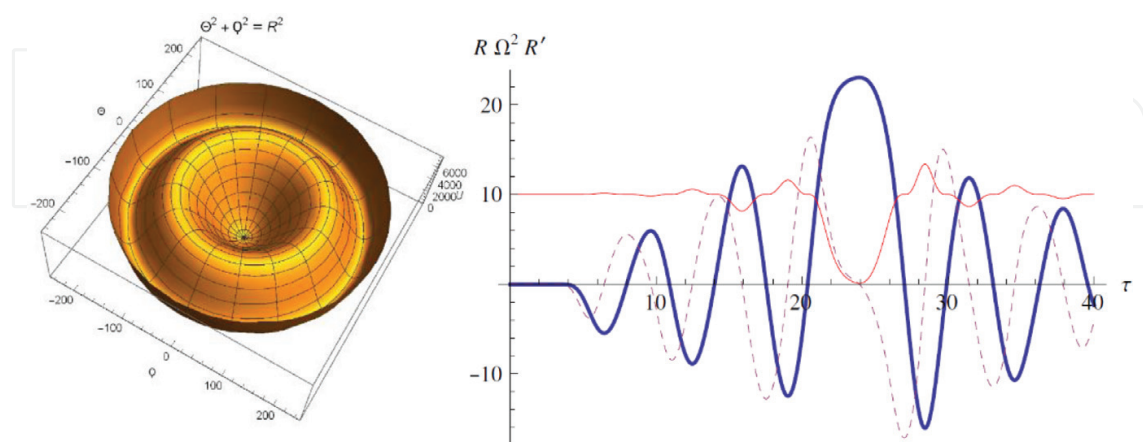
Figure 4. Two-dimensional potential with two minimums which correspond to destroy DNA schemes represented in **Figures 1** and **2**. First minimum corresponds to nondimmer DNA and second minimum to the dimerization of DNA under the UV-C radiation. In the right hand, the transfer of DNA from first minimum to the second minimum is plotted. The thick line represents the behavior of $R(t)$, the red line to nonlinear oscillatory frequency in the relative units Ω^2/Ω_0 and $\tau = t/\Omega_0$.

Local vibration energy of the modes may be coupled by nonharmonic nonlinear term. For example, two vibration modes Q and Θ can be represented as a symmetric function relative to the square value of these normal coordinates:

$$H_0 = \frac{M_q}{2}\left(\frac{dQ}{dt}\right)^2 + \frac{M_\theta}{2}\left(\frac{d\Theta}{dt}\right)^2 + \frac{M_q\Omega_q^2 Q^2}{2} + \frac{M_\theta\Omega_\theta^2\Theta^2}{2} - \kappa_q Q^4 - \kappa_\theta\Theta^4$$
$$- \kappa_{\theta,q}\Theta^2 Q^2 + \chi_q Q^6 + \chi_\theta\Theta^6 + \chi_{q,\theta}\Theta^2 Q^4 + \chi_{\theta,q}\Theta^4 Q^2 \tag{1}$$

Here M_i, Ω_i, and κ_i are the effective mass, frequency, and nonharmonic parameter for the vibration mode i; $\kappa_{\theta,q}$ is the nonlinear coupling of the normal modes of molecule oscillations. The nonharmonic terms present in the Hamiltonian describe the possible inactivation of pathogens at higher excitation.

Two situations of the vibration of this molecular system represented by DNA or tubulins in protein packing in the bacteria microtubule are considered. Collective nonlinear coupled modes, for example, phonons in the condensed mater [31, 32], were introduced and described by the Hamiltonian (1). Therefore, two vibration modes, Q and Θ, become aperiodic according to the theory of catastrophe [33], for higher excitation of the system with short laser pulses [13, 30] with the pulse duration $\tau_L < 1/\Omega_i$:

$$\frac{d^2}{dt^2}Q + \left\{\Omega_q^2 - 4\tilde{\kappa}_q Q^2 + 6\tilde{\chi}_q Q^4 - 2\tilde{\kappa}_{q\theta}\Theta^2 + 2\tilde{\chi}_{\theta,q}\Theta^4 + 4\tilde{\chi}_{q,\theta}\Theta^2 Q^2\right\}Q + 2\Gamma_q\frac{d}{dt}Q = F_q(t);$$
$$\frac{d^2}{dt^2}\Theta + \left\{\Omega_\theta^2 - 4\tilde{\kappa}_\theta\Theta^2 + 6\tilde{\chi}_\theta\Theta^4 - 2\tilde{\kappa}_{q\theta}Q^2 + 2\tilde{\chi}_{q,\theta}Q^4 + 4\tilde{\chi}_{\theta,q}\Theta^2 Q^2\right\}\Theta + 2\Gamma_\theta\frac{d}{dt}\Theta = F_\theta(t). \tag{2}$$

Here, we have introduced the attenuation constant, Γ_i, of each coupling mode through nonlinear interaction, $\tilde{\chi}_{ij} = \chi_{ij}/M_i$; $\tilde{\kappa}_{q\theta} = \kappa_{\theta,q}/M_i$. The nonharmonic term of each mode is described by the nonlinear constant $\tilde{k}_i = k_i/M_i$. The first and second equations of (2) use the corresponding component for anisotropy effective masses M_q and $M\Theta$. The nonharmonic potential is described by the two-dimensional localization potential in **Figures 1** and **4**. If it is absent, the mass anisotropy and two dimensions become symmetrical and we may do the substitution $Q = R\cos\varphi$ and $\Theta = R\sin\varphi$ so that the terms $\left(M_q\Omega_q^2 Q^2 + M_\theta\Omega_\theta^2\Theta^2\right)/2$, $\kappa Q^4 + \kappa\Theta^4 + 2\kappa\Theta^2 Q^2$, and $\chi Q^6 + \chi\Theta^6 + 3\chi\Theta^2 Q^4 + 3\chi\Theta^4 Q^2$ in Hamiltonian (1) can be substituted by $M\Omega^2 R^2/2$, κR^4, and χR^6. Taking into consideration the symmetric form of the Hamiltonian,

$$H_0 = \frac{M}{2}\left[\left(\frac{dQ}{dt}\right)^2 + \left(\frac{d\Theta}{dt}\right)^2\right] + \frac{M\Omega_0^2 R^2}{2} - \kappa R^4 + \chi R^6,$$

we reduce the system of Eq. (2) to a single equation for radial component of nonlinear oscillator

$$\frac{d^2}{dt^2}R + \left\{\Omega_0^2 - 4\tilde{\kappa}R^2 + 6\tilde{\chi}R^4\right\}R + 2\Gamma\frac{d}{dt}R = F(t). \tag{3}$$

Short laser pulses applied externally interact with the molecular dipole of virus components. Consequently, the Hamiltonian takes the traditional form $H_I = -(\mathbf{P}(E), \mathbf{E}(t, z))$. Following the common representation [34–36], the laser field induces the biomolecule polarization, in which components, in similar representation, have tensor character. They depend on the symmetry of excited molecules (virus' or bacteria's constituents) $P_j(E) = \alpha_{jl}E_l$. Because of the tensor character of the two oscillation modes, we can decompose the recognizability $\alpha_{jl}(Q, \Theta)$ in Taylor series relative to the normal components Q and Θ

$$\alpha_{jl} \simeq \alpha_{jl}^0 + \frac{\partial \alpha_{jl}}{\partial Q}Q + \frac{\partial \alpha_{jl}}{\partial \Theta}\Theta + \varepsilon\left(Q^2; \Theta^2; Q\Theta\right).$$

By introducing this expression in the interaction Hamiltonian, we observe that the interaction with the local vibration modes can be described by the function

$$U_I = \alpha'_{jlk}E_jE_lQ_k,$$

where $Q_1 = Q$, $Q_2 = \Theta$, and the tensor $\alpha_{jlk'} = \partial\alpha_{jl}/\partial Q_k$ must be maximally symmetrical according to the symmetry of the virus or bacteria biomolecules. Considering that laser pulses have same polarization, we represent it through the time-dependent Gaussian function $E_i = E_0\exp\left[-\left(t/\sqrt{2}\tau_L\right)^2\right]\cos(\omega_i t)$. For this, we substitute the generalized driving forces $F_j = -\partial U_I/\partial Q_j$ in the system of Eq. (2). The numerical solution of symmetrized nonlinear Eq. (3) for the following expression of the parameters of the potential $2U/\left(|M\Omega_0^2\right) = R^2 - 4.1 \cdot 10^{-5}R^4 + 4.5 \cdot 10^{-10}R^6$ of the system is represented in **Figure 4**. Here, we have used the relative attenuation constant $2\Gamma/\Omega_0 = 10^{-3}$. In case of short laser pulses with relative intensity,

$$F(\tau)/\Omega_0^2 = \sum_1^8 \left[4.7 \cdot \exp\left[-(\tau - 5n)^2\right]\sin(\tau)\right],$$

$\omega_a - \omega_s = \Omega_0$, and $\Omega_0\tau_L = 1$ were chosen as parameters. As follows from the numerical solution of Eq. (3), in the relative time moment $\tau \sim 25$, the nonlinear oscillator achieves the local maximum potential between the wells represented in the left figure of **Figure 4**. After this relative time point ($\tau > 25$), the nonlinear oscillator relaxes in the second minimum of double well potential according to the numerical representation in **Figure 4**. This localized state corresponds to the damage situations of DNA discussed in **Figure 2**.

Let us give the analytical representation of this excitation process described by the system of nonlinear Eq. (2). According to Refs. [13, 29], we observe a same exponential dependence on the $\Omega_j\tau_L$, in the initial stage of excitation $Q_j = Q_{0j}\exp\left[-\Gamma_j t\right]\sin(\Omega_j t)$, when nonlinear frequency is approximated with linear part $\Omega_j(Q, \Theta) \approx \Omega_j$, $j = 1, 2$. Here we consider that $Q = Q_1$ and $\Theta = Q_2$. After the first pulse with duration, $\Omega_0\tau_L \ll 1$, the amplitude has the following dependence on the intensity, E_0^2, pulse duration, τ_L, and local oscillation frequency of the normal mode j, Ω_j

$$Q_{0j} = \frac{\sqrt{\pi}\tau_L E_0^2 \alpha'_j}{2\Omega_j} \exp\left[-(\Omega_j \tau_L)^2/4\right].$$

For simplicity, let us add the next square terms in the system of Eq. (2). As in Refs. [13, 29], we address the problem so as to excite the system of coupling oscillators (2). Consequently, the "nonlinear frequency" $\sqrt{\Omega_q^2 - 4\chi_q\langle Q^2\rangle - 2\chi_{q\theta}\langle\Theta^2\rangle}$ reached zero value, which equals to the termination of the local vibration mode after a finite number of short laser pulses. Let us consider a set of "n" consequent pulses generated in the time interval $T < \Gamma_j^{-1}$. The cumulative energy of the local oscillator after the precursor pulse may be used for the next excitations. For example, after the first pulse, Q and Θ amplitudes of models are described by the expression above. Introducing this expression in the system of Eq. (2), we obtain the following mean values of Q^2 and Θ^2,

$$\langle Q_j^2\rangle = \frac{\pi\tau_L^2 E_0^4 \alpha'^2_j}{2 2^2 \Omega_j^2} \exp\left[-(\Omega_j\tau_L)^2/2\right].$$

In other words, we obtain the new frequencies of nonlinear oscillator modes of the system of Eq. (2) described by linearized differential equations with renormalized frequencies by the first pulse

$$\frac{d^2}{dt^2}O(t) + \left\{\Omega_q^2 - 4\chi_q\langle Q^2\rangle - 2\chi_{q\theta}\langle\Theta^2\rangle\right\}Q + 2\Gamma_q\frac{d}{dt}O(t) = F_q(t);$$

$$\frac{d^2}{dt^2}\Theta(t) + \left\{\Omega_\theta^2 - 4\chi_?\langle\Theta^2\rangle - 2\chi_{\theta q}\langle Q^2\rangle\right\}\Theta + 2\Gamma_\theta\frac{d}{dt}\Theta(t) = F_\theta(t).$$

(4)

The solutions of these equations are similar to expression (2) in which, instead of Q_{0j}, it is used by the new expression;

$$Q(t_2) = Q_{01}\exp\left[-\Gamma_q t_2\right]\sin\left(\tilde{\Omega}_q t_2\right) + Q_{02}\exp\left[-\Gamma_q t_2\right]\sin\left(\tilde{\Omega}_q t_2\right)$$

Here, the second part contains the particular solution of the excitation of oscillator after the second pulse

$$Q_{02} = \frac{\sqrt{\pi}\tau_L E_0^2 \alpha'_q}{2\tilde{\Omega}_q} \exp\left[-\left(\tilde{\Omega}_q\tau_L\right)^2/4\right],$$

where $\tilde{\Omega}_q = \sqrt{\Omega_q^2 - 4\chi_q\langle Q^2\rangle - 2\chi_{q\theta}\langle\Theta^2\rangle}$. This procedure to excite a nonlinear oscillator may continue till one of the amplitudes of oscillation attains the maximal separation line of nonlinear potential function $U_0(Q, \Theta)$, as represented in **Figure 5**. It corresponds to the case when the frequency achieves the zero value after "n" short pulses

$$\Omega_q^2 - 4\chi_q\langle Q_n^2\rangle - 2\chi_{q\theta}\langle\Theta_n^2\rangle = 0;$$

or

$$\Omega_\theta^2 - 4\chi_q\langle\Theta_n^2\rangle - 2\chi_{\theta q}\langle Q_n^2\rangle = 0.$$

In fact, this effect may be observed in a single pulse excitation of nonlinear system of Eq. (2).

The above-described excitation method depends on the condition imputed for applied pulse duration relative to the vibration frequency of biomolecules $\Omega\tau_L < 1$. The local molecular oscillator is described by nonlinear equations; therefore the local frequency depends on the excited energy of such biomolecule. To surpass this difficulty, it is better to consider a longer laser pulse $\Omega\Gamma^{-1} > \Omega\tau_L > 1$, so that during the excitation to apply for selective excitations of virus and bacteria (see **Figure 5**). This excitation method is alike to the diagnostics of molecular systems suggested in Refs. [14–16]. The method attracted many specialists in CARS diagnostics and studies of molecular and cellular subsystem design. According to this theory, the strength product [5] of two possible fields through the Stokes and anti-Stokes generation components is introduced:

$$\Pi^-(t, z) = E_p^+(z, t)E_a^-(z, t) + E_s^+(z, t)E_p^-(z, t)$$
$$= G(k_p, k_a)\hat{b}\hat{a}^\dagger\exp\left[i\Omega_0 t - i(k_a - k_p)z\right] + G(k_s, k_p)\hat{s}\hat{b}^\dagger\exp\left[i\Omega_0 t - i(k_p - k_s)z\right], \tag{5}$$

Here, $E_p^+(z, t)$, $E_s^+(z, t)$, and $E_a^+(z, t)$ are the positively defined pump, Stokes, and anti-Stokes strength components of Raman process, expressed by the generation of photon operators in each mode $\hat{b}^\dagger$, $\hat{s}^\dagger$, and $\hat{a}^\dagger$, respectively. The related negative field component expressed by the annihilation operators is introduced in expression (5). The frequency $\Omega_0 = \omega_p - \omega_s = \omega_a - \omega_p$ is approximately equal to local vibration mode of the biomolecule Ω. Accordingly, the interaction Hamiltonian with the local nonlinear mode of viruses or bacteria may be described by:
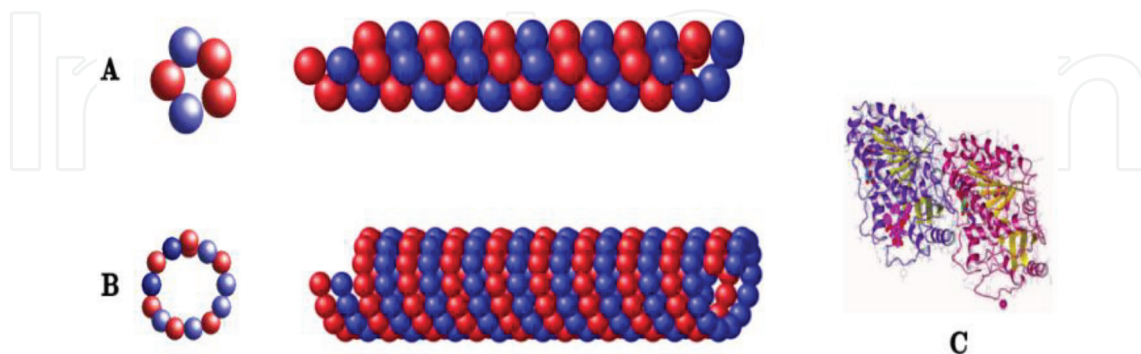
Figure 5. Comparison of 5-protofilament bacterial microtubule architectures. (A) α and β tubulins are represented in blue and red, respectively. (B) Representation of a 13-protofilament eukaryotic microtubule: α—tubulin in red; and β—tubulin in blue. Seams and start-helices are indicated in green and red, respectively. (C) The biomolecular structure of α and β tubulins is indicated.

$$\hat{H}_I = -\hat{\Phi}^+(t,z)\hat{\Pi}^-(t,z) + H.c., \tag{6}$$

The operator $\hat{\Phi}^+(t,z)$ is proportional to the displacement of local oscillator mode from the equilibrium position, $\hat{P}(t,z) \sim \hat{Q}(t,z) \sim |e><g| + |g><e|$. The two-mode Raman transitions from the first excited to the ground states of the local oscillator are given in **Figure 6**.

Bistable excitation process of nonlinear oscillator in external biharmonic field was in the center of attention in many papers (see, e.g. [34, 37]). Following the ideas of Ref. [37], we simplify the local vibration system (2) to single vibration mode Q described by the nonlinear Hamiltonian:

$$\hat{H}_0 = \hbar\Omega\hat{q}^\dagger\hat{q} - \hbar\kappa(\hat{q}^\dagger)^2(\hat{q})^2 \tag{7}$$

Introducing the new excitations, $\hat{D}^+ = \hat{q}^\dagger\sqrt{\Omega_0/\kappa - \hat{q}^\dagger\hat{q}}$, and de-excitation, $\hat{D}^- = \sqrt{\Omega_0/\kappa - \hat{q}^\dagger\hat{q}}\hat{q}$ operators in the vibration mode of the nonlinear Hamiltonian (6) [38], we observe that their commutation relation $\left[\hat{D}^+, \hat{D}^-\right] = 2\hat{D}_z$. For biomolecules with a positive nonharmonic parameter $\kappa > 0$, we observe that the inversion $\hat{D}_z = -\Omega_0/(2\kappa) + \hat{q}^\dagger\hat{q}$, together with two x and y polarization components, $\hat{D}_x = \left(\hat{D}^+ + \hat{D}^-\right)/2$ and $\hat{D}_x = \left(\hat{D}^+ - \hat{D}^-\right)/2i$, forms the square pseudovector $\hat{D}^2 = \hat{D}_z^2 + \hat{D}_x^2 + \hat{D}_y^2$, which is conserved during the excitations. These operators are similar to angular momentum generators in quantum mechanics and belong to $SU(2)$ algebra. Similar operators can be introduced for bimodal field in Raman scattering (7), $\hat{L}_z = \hat{a}^\dagger\hat{a} - \hat{s}^\dagger\hat{s}$; $\hat{L}^- = \sqrt{2}\left(\hat{b}\hat{s}^\dagger + \hat{a}\hat{b}^\dagger\right)$; $\hat{L}^+ = \sqrt{2}\left(\hat{s}\hat{b}^\dagger + \hat{b}\hat{a}^\dagger\right)$. Here, in rotating wave approximation, we obtain the following symmetrical form of the Hamiltonian:

$$\hat{H} = \hbar\Delta\hat{D}_z - \hbar\kappa\hat{D}^+\hat{D}^- - \hbar g\left\{\hat{L}^-\hat{D}^+ + \hat{D}^-\hat{L}^+\right\}, \tag{8}$$

which describes the interaction of three discrete modes of microcavity (or nanofiber) with nonlinear vibration of biomolecule with conservation of total number of photons and two pseudovectors, D^2 and $L^2 = \hat{L}_z^2 + \hat{L}_y^2 + \hat{L}_x^2$. In the Hamiltonian (8), we have $\Delta = \Omega - \Omega_0$, which is the detuning from resonance to the frequency of bimodal vector of Raman field, Ω_0, and the frequency of local oscillator, Ω. κ is the nonharmonic parameter, which drastically reduces the distance between the level of harmonic vibrations of the molecular system. The coupling constant $\hbar g$ describes the biharmonic coupling between the vibrational mode of biomolecules and Stokes, pump, and anti-Stokes modes of the electromagnetic field. Let us study the case when $\Omega\tau_L > 1$ and the damping rate of excited oscillator is lesser than life time of Stokes, anti-Stokes, and pump photons in nanofibers. Here, the operators of electromagnetic field in the density matrix of the system might be adiabatically eliminated. If we consider that the photons are organized in the anti-Stokes mode, we obtain a master equation, which characterizes the dynamic behavior of biomolecule nonlinear oscillators:

$$\frac{\partial}{\partial t}\hat{W}(t) = -i\left[\Delta\hat{D}_z, \hat{W}(t)\right] + i\kappa\left[\hat{D}^+\hat{D}^-, \hat{W}(t)\right] + \left\{i\Omega_R\left[\hat{D}^+\hat{W}(t)\right] + \left[\hat{D}^-\hat{W}(t), \hat{D}^+\right] + H.c.\right\}, \quad (9)$$

Here $\Omega_R \simeq g\sqrt{2n_a n_p}$ and $\gamma \approx 2g^2 n_a \varepsilon/(\Delta^2 + \varepsilon^2)$ are the two-photon Rabbi frequency and the coherent scattering rate of the applied anti-Stokes field component, while n_a and n_p are the numbers of photons in the anti-Stokes and pump modes. When detuning Δ is positive, the excitation of nonlinear oscillator is compensated by the nonharmonic term in the master Eq. (9), which is proportional to the nonlinear parameter, κ. This excitation is complemented by the improving of resonance between the excited vibration levels of molecular oscillator. It may be defined as a jump of the number of excitations with increasing of the external field intensity. Using the solution of the equation, the number of excitations of the nonlinear oscillator can be given as a function of intensity of applied field Ω_R, nonlinear parameter κ, and detuning from resonance Δ:

$$n = \frac{N}{2} - \sum_{n=0}^{N} n\frac{\Gamma(N+n)}{\Gamma(2n)\Gamma(2j-n)}\left\{\frac{\left|\Gamma\left(1 + i\tilde{\delta} + n\right)\right|^2}{\tilde{v}^{2n}\left|\Gamma\left(1 + i\tilde{\delta}\right)\right|^2}\right\}\frac{1}{2A}. \quad (10)$$

The normalized constant is

$$A = \sum_{n=0}^{N}\left\{\frac{\left|\Gamma\left(1 + i\tilde{\delta} + n\right)\right|^2}{\left|\tilde{v}2n\right|\Gamma\left(1 + i\tilde{\delta}\right)\right|^2}\right\}\frac{\Gamma(N+n)}{\Gamma(2n)\Gamma(2j-n)}. \quad (11)$$

Here, $\tilde{\delta} = \delta(1 + i\chi)/(1 + \chi^2)$; $\tilde{v} = v/(1 + i\chi)$, where the new parameters represent the relative values of the detuning $\delta = \Delta/\gamma$; nonlinear parameter $\chi = \kappa/\gamma$, and the intensity of the field $v = \Omega_R/\gamma$.
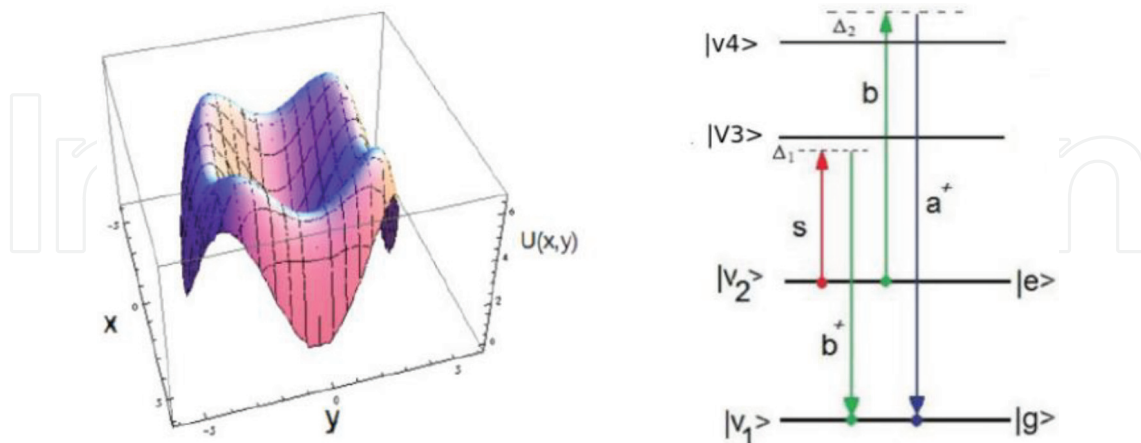
Figure 6. The dependence of the potential energy of the nonlinear oscillator on two normalized modes $x = \sqrt{M/2\Omega}Q$ and $y = \sqrt{M/2\Omega}\Theta$, energy scheme for such nonlinear potential with possible Raman excitation. Reproduced with permission from [6].
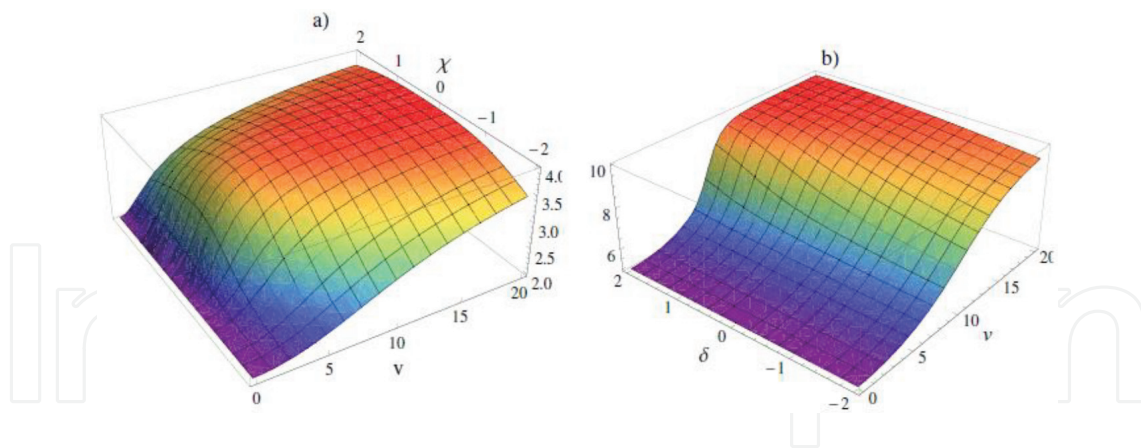
Figure 7. The dependence of number of excitation n as function of (a) coherent excitation, ν, and nonlinearity, χ, for constant detuning, $\delta = 2$, and (b) coherent excitation, ν, and detuning, δ, for the constant nonlinearity, $\chi = 2$. Here, the total number of excitation is $N = 10$. Reproduced with permission from [6].

The number of excitations for a nonlinear oscillator is defined by the ratio $N = \Omega/\kappa$. Following the solutions (10) presented in literature in various publications (see, e.g. Ref. [37]), we displayed in **Figure 7** the mean number of excitations as a function of the intensity and nonlinearity of applied field or as a function of excited field and detuning. This phase transition is typically described by a bistable behavior of the nonlinear oscillator. Taking into account other nonlinear terms (e.g., Q^6) in the Hamiltonian (1), we may terminate the nonharmonic oscillator moved to other metastable position.

3. Decontamination volume estimated for different metamaterials

Latest investigations consider the geometry of metamaterial elements for different applications [38–43]. Conical metallic nanoparticles in an array configuration could be used for localization of SPR [38]. The geometry of nanoparticles and their arrangement improve the biochemical sensing and detection for drug delivery, heating therapy, etc. Ref. [40] describes a similar localized SPR. An electromagnetic sensor made of nonspherical gold nanoparticles deposited on a silica substrate having a matrix configuration with the interparticle distance much smaller than the incident wavelength is proposed. Other applications of the different geometry of elements of metamaterials are related with optical proprieties of each element. Explicitly, the cylindrical elements of metamaterials could be used as a performing resonator in the optical cloaking [41]. The authors of Ref. [42] mentioned that macroscopic characteristics depend not only on molecular structure but also on specific geometry. Advances and potential applications of optical electromagnetic metamaterials and metasurfaces for refractive index sensing and sensing light properties are presented in Ref. [43]. These metamaterials can be simply integrated with several electronic devices.

Here, we give a clear explanation for the increasing of the penetration depth of UV-C radiation inside the decontamination core. It is due to multiple refractions and reflections of radiation on the spherical and conical structures of metamaterials. If the light enters into the translucent liquid through a circular surface, the decontamination volume may be proportional to the surface of the

circle multiplied by the attenuation depth of the radiation inside the contaminated liquid (see **Figure 8**). Conversely, if the light penetrates the liquid through the base of a quartz semisphere, the contact surface increases two times, becoming $2\pi R^2$. The decontamination volume also increases, becoming equal to the surface of semisphere multiplied by attenuation depth. If the light is introduced inside the cone through its base, a considerable increase of the contact surface metamaterial (liquid) occurs. Here, the multiple refractions of UV-C radiation inside the cone improve the contact surface between the quartz cone and the translucent liquid. It increases significantly when the cone generator is larger than the cone radius. The multiple optical contacts between metamaterial elements (spheres, granules, conic elements, fibers) lead to a drastically dispersed light inside the contaminated fluid that flows between these elements.

Let us analyze the liquid decontamination by traditional method, which makes use of UV-C pulsed light (see **Figure 9(a)**). If the contaminated liquid flows inside a cylinder and it is irradiated from all directions with UV radiation, the total decontamination surface is $S = 2\pi R(L + R)$. The first term designates the lateral surface, the last term the surface of the bases, R the radius of the base, while L is the length of the cylinder. Using classical decontamination, a large volume, V_{con}, of infected liquid remains contaminated:

$$V_{cl} = \pi 2\pi R(L + R)d_p;$$

$$V_{con} = \pi R^2 L - V_{cl} \gg V_{cl},$$

where V_{cl} represents the efficient decontamination volume and $d_p \sim \lambda$ is the UV radiation penetration depth into liquid. Further down, we suggest a decontamination method making use of metamaterials in order to increase the decontamination volume.

Sensing properties are anticipated to be related to nanoscale system dimensions. In a first step, the contact surface of flowing gas or liquid is estimated. To increase the contact surface of the contaminated liquid, we examined the UV radiation propagation in two types of metamaterials: type A corresponds to the packing of photonic crystal fibers (PCFs) and type B to the photonic crystals (PCs) (see **Figure 9(b** and **c)**). Both metamaterials are transparent in UV region.
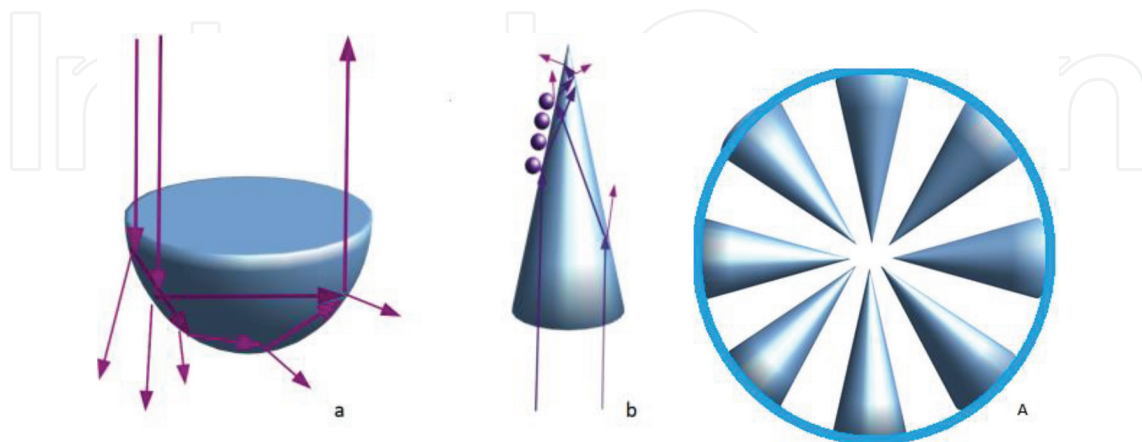
Figure 8. The multiple reflection and refractions of the UV light passing through the bases of semispherical (a) and conical (b) elements of metamaterial. Figure A represents the decontamination core filled up with conical structures. The radiation of six UV lamps is guided inside the center of decontamination tube through the bases of such conical structures where the nontransparent contaminated liquid has the maximal flow velocity.
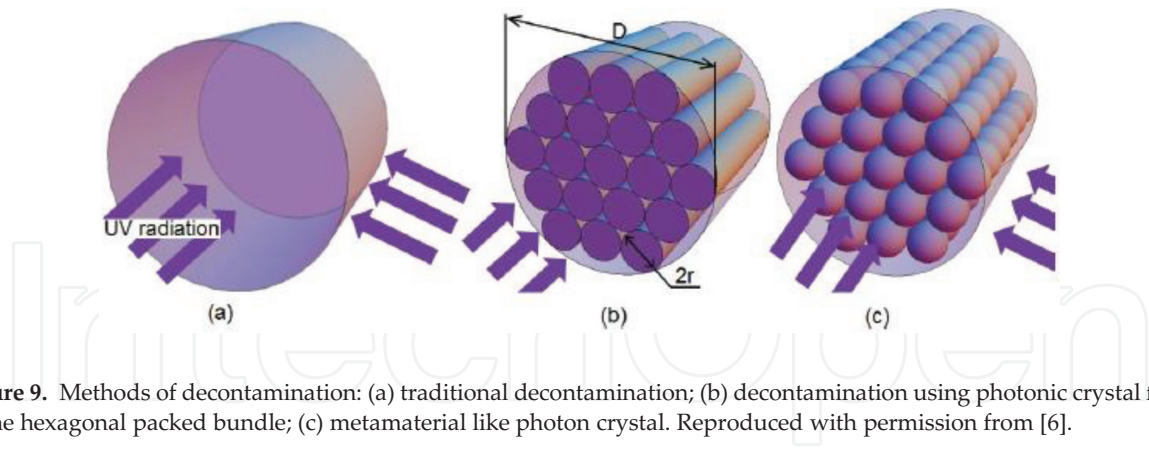
Figure 9. Methods of decontamination: (a) traditional decontamination; (b) decontamination using photonic crystal fibers in the hexagonal packed bundle; (c) metamaterial like photon crystal. Reproduced with permission from [6].

When the PCF system is positioned in a cylinder containing contaminated liquid (see **Figure 9(b)**), this liquid will fill completely the space between fibers. Therefore, the decontamination surface grows substantially

$$S_d = \pi r(r + 2rLN), \tag{12}$$

where N is the number of fibers from PCF and r is the radius of one fiber. Last term stands for the fibers' lateral surface. It is assumed that the UV radiation is introduced by fibers in the cylinder. The UV radiation penetration depth (evanescent field) is influenced by the relative refractive indexes of fibers and contaminated liquid. The evanescent field intensity is given by:

$$I = I_0 \exp\left[-z/d\right], \tag{13}$$

where I is the intensity of evanescent zone at distance z from fiber and d is characteristic exponential decay depth expressed as:

$$d = \frac{\lambda}{4\pi n_2} \sqrt{\frac{\sin^2(\theta_c)}{\sin^2(\theta) - \sin^2(\theta_c)}}.$$

Here, θ_c represents the critical angle of incidence $\sin\theta_c = n_2/n_1$, θ is the angle of incidence, $\theta > \theta_c$; n_1 is refractive index of the fibers, n_2 is refractive index of the liquid medium, while λ is the wavelength of UV radiation. In order to connect this approach with the classical decontamination method, it is necessary to indicate the decontamination area through the number of fibers. The estimates show that the small radius of fiber r is proportional to $r \sim R/\sqrt{N}$. If r is introduced in relation (12), the decontamination area of N cylindrical fibers is obtained:

$$S_d \sim 2\pi RL\sqrt{N}. \tag{14}$$

According to (14), the decontamination surface is proportional to the square root of N, number of fibers. Here, we consider negligibly the small surfaces of cylinder base as compared with the lateral surface of the fibers. Eqs. (13) and (14) demonstrate that decontamination volume of liquid is, in this case, proportional to

$$V_d \sim 2\pi RLd\sqrt{N} \tag{15}$$

It is obvious also that the decontamination volume is proportional to $\sqrt{N}$ ($V_d/V_{cl} \sim \sqrt{N}$). But it is yet not clear what happens with the free volume of liquid flowing between fibers, which is placed at a bigger distance in comparison with $\lambda/2$. This volume may be implicated in the contamination zone if the thickness of the fiber is decreased.

Using a standard hexagonal packed bundle symbolized in **Figure 9(b)**, it is possible to estimate the free volume between three fibers $v_f = r^2(\sqrt{3} - \pi/2)L = 0.18r^2L$. In this case, the free volume in the big bundle does not depend on the diameter of the fiber and is equal to $V_f = \pi R^2 L(\sqrt{3} - \pi/2)$. The unused volume may be expressed as $V_a = \pi RL(0.18R - \sqrt{N}\lambda)$. When this expression reaches zero value, the whole volume between the fibers can be used for fluid decontamination. Consequently, the fiber radius is $r \sim R/\sqrt{N} \sim \lambda/0.18$. A similar expression can be obtained for other types of fiber packing. Using the same method, we have estimated the decontamination surfaces of metamaterials like PC (see **Figure 9(c)**).

$$S_d = 4\pi r^2 N \sim \pi L^2 N^{1/3},$$

where L is the edge length of the cube, r is the radius of one microsphere, and N is the number of microspheres of the metamaterial. The liquid fills the space between microspheres and the decontamination volume can be expressed as

$$V_d \sim dS_d = 4\pi dR^2 N^{1/3} \tag{16}$$

We mention here that the increase of decontamination volume depends on the number of microspheres, described by a $N^{1/3}$ dependence.

At a first glance, it appears that the decontamination volume is smaller than in PCF, but this is just an illusion. Because the number of microspheres in a PC-like metamaterial is much larger than the number of fibers in PCF, decontamination volume is much higher in the second case. Another priority of last metamaterial consists in the fact that this works in all directions symmetrically, in comparison with PCF.

The free volume between spheres in a PC can be expressed as $v_{fr} = (2r)^3 - 4(\pi r^3/3) = 8r^3$ $(1 - \pi/6) \sim 0.48 v_c$. The free volume between large cubes with dimension L have the same proportion $V_{fr} = 0.48V$. In this case, the difference $V_{fr} - V_d$ is proportional to $V[0.1/3/(2L)]$. When $L < \pi N^{1/3}/0.98$, a further increase of surface becomes impossible and therefore the classical aspect of evanescent zone is not acceptable. Consequently, the volume between the spheres may be considered a decontamination zone.

Metamaterials, as optical fibers or periodic photonic structures, open new possibilities to manipulate and annihilate viruses and bacteria in contaminated areas of liquids or organic tissue. For example, a good contact area between the implant and cells can be obtained if such metamaterials will cover the surface. The UV radiation guided along the surface of the implant ensures the best medical support against potential viruses or bacteria.

The depth and the volume of the evanescent zone of periodical waveguide structures influence UV action against bacteria and viruses. In **Figure 10**, we represent a periodical structure

(containing fibers and spherical metamaterials), which is introduced in a cylinder inside the contaminated fluid flows. Using Eqs. (12), (15), and (16) (arrangements (b) and (c) in **Figure 9**), the relative decontamination coefficient is introduced:

$$\rho = \frac{V_d}{V_c}.$$

Since the cylinder has a lateral surface larger than that of the bases, the relative decontamination coefficient is $\rho \sim d\sqrt{N}/d_p$. A similar expression can be written for PC-like metamaterials if the cylinder is filled up with SiO_2 periodical bubbles. For this, the relative decontamination coefficient is $\rho \sim dN^{1/3}/d_p$. The classical decontamination volume is considered to be the penetration of radiation into the spherical elementary volume $4\pi R^2 d_p$ with the width $\Delta R \sim d_p$. Periodical fiber structures and periodical spherical materials were proposed for carrying out the preliminary measurements in decontamination procedures as a function of the intensity and pulse duration of UV pulses.

Taking this dependence into consideration, we used a funnel filled with 400 fibers. The relative coefficient, ρ, of contaminated liquid, which flows through the funnel filled up with fibers and a funnel without fibers for the same flowing volume, is calculated. This coefficient becomes 20 times larger for the same volume of liquid flowing inside the cylindrical part of the funnel filled with fibers (relative to funnel without fibers), when the penetration depth is comparable with the depth of the evanescent field $d \sim d_p$, where $d \sim 100$ nm. A similar equipment for SiO_2 cylinder filled with SiO_2 spherical bubbles through which contaminated liquid flows under the intense UV irradiation delivered by six lamps (see **Figure 10**) is proposed and preliminary tested. The decontamination rate is proportional to $N^{1/2}$ for PCF and to $N^{1/3}$ for PC, respectively.

Our previous studies [4] were devoted to the research of chemical reactions, which are produced in the microorganisms under UV pulse action. Here, one should consider the quantified structure of a quasiparticle energy transmitted from one DNA segment to another, or connected to protein microtubule. These vibration structures are analogous with two-dimensional phonon flows,
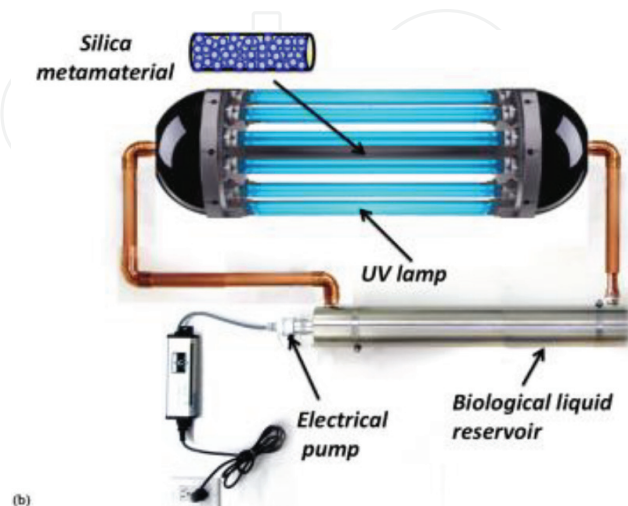
Figure 10. Experimental schemes proposed for the improvement of UV radiation contacts with fluids in the periodic optical SiO_2 structures in interacting with the contaminated liquids. Reproduced with permission from [6].

which are studied in graphene, boron nitride, or planar superlattices [31]. During decontamination process, the trapping of pathogen particles (viruses and bacteria) near the surface of fibers (or spheres) can occur. This effect was also described in literature [44]. It involves the attractive force acting on the particles presenting higher refractive indexes relative to the refraction index of liquid. This force occurs as a consequence of the large gradient of electromagnetic field (EMF) in the evanescent zone nearby the fiber (sphere).

In the next section, the contact area between the radiation propagating through the metamaterial elements and contaminated translucent fluids is increased. The decontamination rate is proportional to periodical spherical structures (N stands for the number of metamaterial elements) [4–6]. The efficiency of UV-C action on microorganisms present in contaminated fluids depends on the depth and volume of the evanescent zone of periodical waveguide structures.

4. Experimental decontamination equipment with metamaterials

For the decontamination of translucent liquids by UV-C radiation, we proposed the equipment in **Figure 11**, formed from a UV-C transparent core tube, which can be filled with metamaterials. As was estimated in Section 3, the decontamination rate is influenced by the packing and optical properties of metamaterial elements. Two types of metamaterials were used: (a) quartz (SiO_2) unordered granules with dimension around 1–5 mm and (b) transmission spectrum in UV region 240–260 nm (**Figure 11(a** and **b)**) spheres of glass material with diameter of 2 mm and transmission at 300 nm. The comparative analysis of the decontamination rate for these metamaterials is performed. Optical metamaterials can disperse UV-C light inside the fluid volume and improve the contact zone between radiation and contaminated fluids. In **Figure 11(a)**, the UV-C core tube used for the decontamination of translucent fluids is shown, while **Figure 11(b)** presents the decontamination equipment for dynamic treatment regime. The decontamination equipment consists of six low-pressure Hg UV-C lamps (30 W) with 90 cm length and about 2.7 cm diameter. These lamps surrounding the decontamination core tube (**Figure 10**) are placed in the center of a reflecting aluminum cylinder (with a diameter of about 30 cm). The UV-C radiation (with Gaussian distribution) is focused along the axis, i.e., in the decontamination area. The core tube can be filled up with optical metamaterials, while polluted fluids can freely circulate between elements, in interaction with evanescent waves.

The radiation penetration into the core tube offers a significant yield of the contact surface between the flowing fluid and UV radiation in a volume of $\sim 0.9 \times 10^{-4}$ m^3. The fluid circulating through the decontamination zone changes arbitrarily the optical frontiers among metamaterial elements and fluid, in function of pathogen concentration and optical properties. Consequently, the decontamination efficiency depends on the contact surface between the contaminated fluid and periodical optical metamaterial, and it is proportional to the number of elements of metamaterial. The penetration of light radiation into translucent fluids flowing through elements of metamaterials increases due to the optical evanescent field around each element. For the dynamic treatment regime, the core tube is connected to an external reservoir through which the polluted biological fluid flows. The circulation of the fluid is conducted by an electrical pump device. The working principle of the installation can be described as follows. The UV-C irradiation
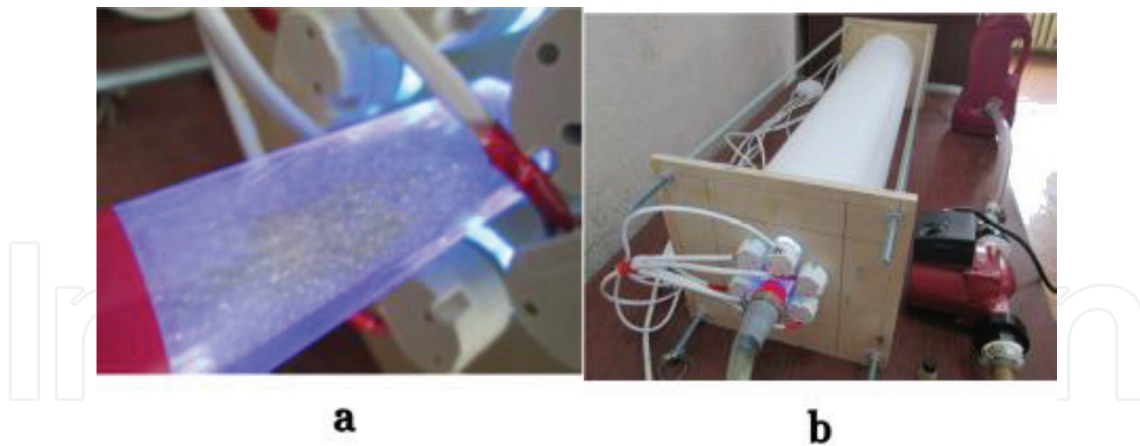
Figure 11. (a) Optical metamaterial used for decontamination and (b) decontamination equipment used for dynamic treatment regime.

of six germicidal lamps is concentrated in the quartz core tube and propagates inside the whole volume through UV transparent metamaterial elements. When using quartz metamaterials, the decontamination volume can be increased by the evanescent zone of UV light radiation forming around each element of the metamaterial.

The microorganism decontamination is achieved in the evanescent area, which can improve the contact zone between radiation and contaminated fluids. The optical force produced by electromagnetic radiation acts as a tweezer, attracting microparticles at the EMF regions with the highest intensity. Microorganisms located in the evanescent zone of metamaterials can be efficiently annihilated. It is worthy to mention that such a UV-C decontamination equipment can be used, as for example, in water distribution system of a city or directly in water pipes of apartments, in order to prevent the biological risk. Moreover, UV-C decontamination reactors can be used for gases (air) decontamination in hazardous situations.

5. Decontamination in dynamic treatment regime

Contaminated water samples collected from metropolitan "Valea Morilor" Lake from Chisinau and sweetened beer yeast solutions were tested. Experiments confirmed that the proposed optical metamaterials effectively disperse the UV radiation inside the liquid volume, improving the contact surfaces between the radiation and liquid. The packing symmetry and optical properties of the metamaterial elements, as well as the optical properties of contaminated liquids influence the decontamination rate.

5.1. Bacteria and fungi inactivation during a dynamic treatment regime

A series of experiments for decontamination of polluted water samples were carried out. The collected lake water samples, contaminated with *Coliform* (including *Escherichia coli*) and *Enterococcus* bacteria, were treated in a dynamic regime for 5 and 10 min. The contaminated

water for testing was pumped by an electrical device to continuously circulate through the core tube filled up with optical metamaterials (glass spherical bubbles). As follows from experimental results (**Table 1**), *E. coli, Enterococcus*, and *Coliform* bacteria were totally inactivated from a volume of 1 L of contaminated water after 10 min of UV-C irradiation in the presence of glass spheres. This keeps valid after 5 min of treatment, as the bacterial colonies of *Coliform* and *Enterococcus* were also annihilated. Nevertheless, an insignificant part of *Coliform* bacteria survived after 5 min irradiation in dynamic treatment (**Figure 12**) (see also **Table 1**). The individual numerical values of the control and treated water samples are collected in **Table 1**.

In **Figure 12**, images of Petri dishes with bacteria colonies after 48 h of incubation are given. Bacteria in the contaminated water that flows in-between the metamaterial elements in the core tube (glass spheres) are periodically collapsed on the evanescent zone of each element.

As can be observed from **Figure 12** and **Table 1**, the *Coliform* (including *E. coli*) and *Enterococcus* bacteria from a volume of 1 L contaminated water were totally inactivated after 10 min of treatment under UV-C irradiation in dynamic regime, in the presence of glass spheres. The contaminated water is penetrated by UV-C radiation via evanescent field around spheres inside the quartz tube cylinder. The decontamination effect is significant in all cases, leading after 10 min to the eradication of all bacterial strains (*B. coliform, E. coli*, and *Enterococcus*).

5.2. Yeast inactivation by dynamic treatment regime

Next experiments were conducted with beer yeast fermentation. The yeast species transforms by fermentation carbohydrates to carbon dioxide and alcohols [45]. The fermentation was used to estimate the decontamination rate efficiency of the UV-C equipment (**Figure 13**).

About 50 g of fresh yeast were dissolved into 1 L of warm (40°C) sweetened water (20%). After 1 h of observation, the fermentation is still active in the untreated solution (**Figure 13B)**, while

| Bacterial strain	Results [CFU/100 cm^3]
Polluted lake water—control samples	
B. coliform	482
E. coli	3
Enterococcus	11
Lake water UV irradiated for 5 min in the core tube filled up with glass spheres	
B. coliform	5
E. coli	0
Enterococcus	0
Lake water UV irradiated for 10 min in the core tube filled up with glass spheres	
B. coliform	0
E. coli	0
Enterococcus	0

Table 1. Characteristic numerical values of untreated (control) and treated water samples in dynamic regime for 5 and 10 min.

in the irradiated one (1 L), during 15 min of circulation through the core tube filled up by unordered granulated quartz (transparent to 254 nm), the fermentation is completely stopped (**Figure 13A)**. These experiments demonstrated that yeast solution treated for 15 min in dynamic regime was efficiently inactivated. Only 5 min irradiation of yeast solution using unordered granulated SiO_2 induced the partial stopping of bubbling in the treated solution, relative to the control samples.

(a)   *(b)*   *(c)*

(d)   *(e)*   *(f)*
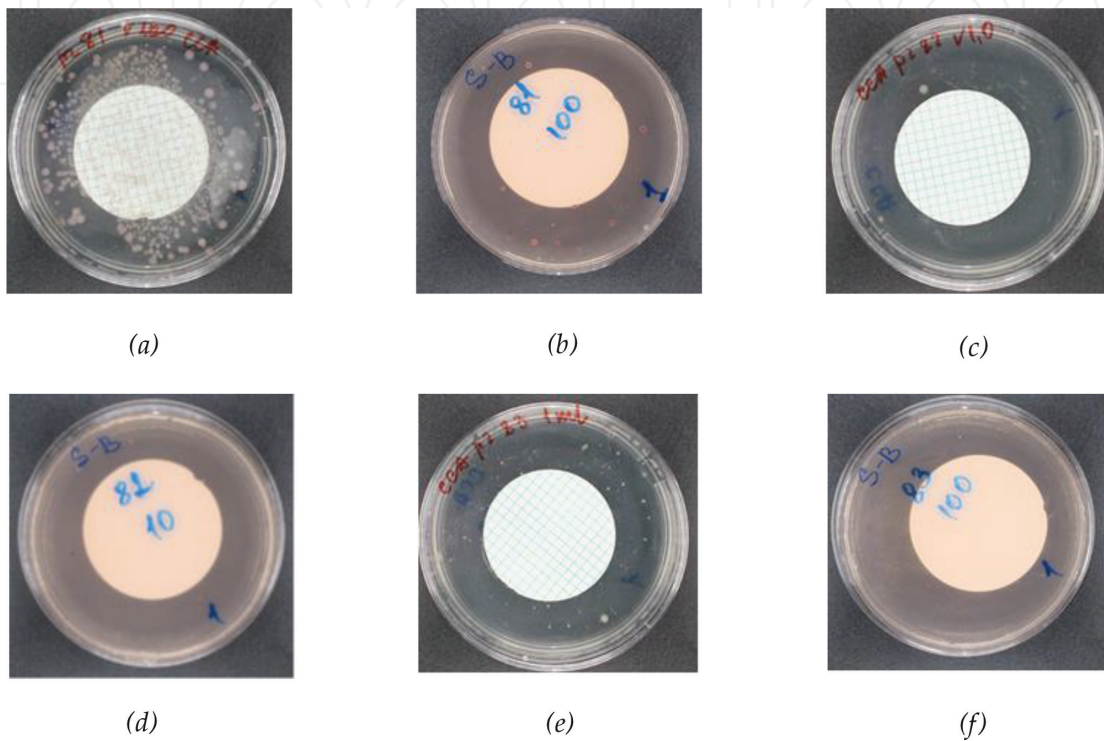
Figure 12. *Coliform bacteria* (inclusively *E. coli*) (a) and *Enterococcus* (b)—control samples, at 48 h growth without UV treatment, irradiated for 5 min (c and d) and irradiated for 10 min (e and f).
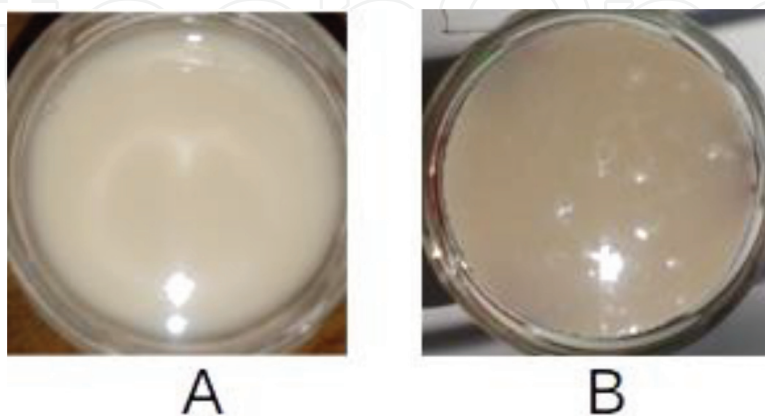
Figure 13. After 1 h, it was observed the stopping of bubbling in the yeast-treated solution (A), while in the untreated solution, the fermentation continued to be active (B).

The fermentation is, however, more active when glass bubbles (approximately 2 mm in diameter) were used in the decontamination equipment. After 5 min exposure, a substantial inhibition of the fermentation was not observed when using glass metamaterials (nontransparent to either UV or visible light).

6. Decontamination in static treatment regime

In order to distinguish between fluid dynamical effects produced as an effect of the acceleration and rotation of microorganisms in polluted fluids, some tests were conducted in static decontamination regime. For this purpose, the decontamination equipment was placed in vertical position. The liquid is motionless in the core tube. The contaminated liquid was UV-C irradiated and crossed by the evanescent field of each element of metamaterial placed in the quartz cylinder. Two dedicated series of experiments were performed in static treatment regime of decontamination: (i) one devoted to annihilation of *E. coli* bacteria in water samples prepared in the Laboratory of Sanitary Microbiology at the National Center of Public Health, Republic of Moldova, and (ii) another to the prevention of mat formation in *Kombucha* culture.

6.1. *E. coli* inactivation in static treatment regime

Water samples contaminated with *E. coli* were treated in static regime by UV-C radiation for 1, 1.5, and 2 min. In **Table 2**, the characteristic numerical values of the nonirradiated (infected with *E. coli*) and irradiated water samples in static regime are collected.

The infected water with *E. coli* was poured in the decontamination "core tube" and was UV-C irradiated for 1 min. In **Figure 14**, the experimental results for decontamination of water samples in static treatment regime using quartz granules in the core tube (**Figure 14B**) and in absence of metamaterials are presented (**Figure 14C**)—corresponding to the traditional decontamination method, see Section 3). For reference, in **Figure 14M**, the photo of Petri dish of the control (untreated) sample is shown.

Nr.	Tested samples, experimental results	Measurement units	
		CFU/ml	CFU/100 ml
E. coli ATCC 25922 with the concentration 10^2 UFC/ml (sample nr. 1)			
1.	Control sample—untreated water contaminated with *E. coli* (reg. nr. 137)	1.9×10^2 CFU/ml	1.9×10^4 CFU/100 ml
2.	Sample nr. 1 water contaminated with *E. coli* treated without metamaterials (reg. nr. 144)	0 CFU/ml	1.6×10^1 CFU / 100 ml
3.	Sample nr. 2 water infected by *E. coli* treated with quartz unordered granules (reg. nr. 143)	0 CFU/ml	0 CFU/ml

Table 2. Characteristic numerical values of the untreated water samples (1) prepared in Laboratory of Sanitary Microbiology at the National Center of Public Health, Republic of Moldova, and the treated water samples without metamaterials (2) and with metamaterials (quartz unordered granules) (3).
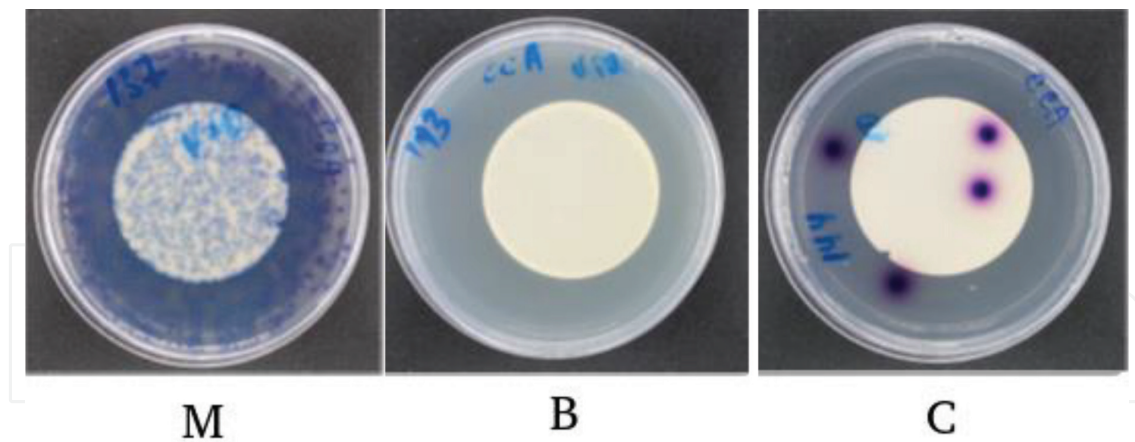
Figure 14. Specially prepared *E. coli* contaminated samples. (M) control sample; (B) sample after static treatment using quartz unordered granules in the core tube; (C) sample after static treatment without metamaterials.

It is observed that *E. coli* bacteria in the samples treated using metamaterials consisting of quartz unordered granules were completely inactivated. On the other hand, for the samples treated without metamaterials, the bacteria were not completely inhibited (**Figure 14**C). In this case, some *E. coli* colonies are still present in the decontaminated liquid. This convincingly demonstrates the key role of quartz metamaterials in liquid decontamination under UV-C irradiation.

6.2. Inactivation of Kombucha tea under static treatment regime

Static decontamination regime was applied to examine samples of *Kombucha* tea, *Medusomyces gisevii* [46]—symbiotic culture of acetic acid—producing bacteria and yeast (Symbiotic Community Of Bacteria and Yeast—SCOBY). They contain one or several species of bacteria and yeast, which form a zoogloeal mat [47], known as "mother" [46]. After a storage period at a temperature higher than 20°C for about 3 weeks, a microbial biofilm is appearing onto the surface of the fermented *Kombucha* tea. It usually has the aspect of a giant oily pellicle. This dense microbial mat is fused together by cellulose produced by bacteria primarily responsible for the glued community. Yeast living in biofilm uses tea sugars to produce alcohol, which is then consumed by neighboring bacteria to produce acetic acid. The yeasts that can form a *Kombucha* culture are *Saccharomyces cerevisiae, Brettanomyces bruxellensis, Candida stellata, Schizosaccharomyces pombe,* and *Zygosaccharomyces bailli* [48]. The bacterial component of *Kombucha* consists of several species but always includes *Gluconacetobacter xylinus* (*G. xylinus*, formerly *Acetobacter xylinus*). *Kombucha*-fermented tea samples were prepared as follows: sugar (10%) is added to the fresh black tea and then a 1:1 quantity to 1-month-fermented *Kombucha* tea, which presents already a dense microbial biofilm on the surface. The UV-C irradiation time was set at 5, 7, 9, or 11 min. The core tube of the decontamination equipment was filled out with (1) granular unordered quartz of 1–5 mm transparent to 254 nm or (2) glass spheres nontransmitting at 254 nm. In the third case, the core tube was kept empty, without metamaterials—the case that models the traditional decontamination method (see Section 3). In *Kombucha* black tea at room temperature, colonies of bacteria (15×10^3 CFU/mL) and yeast (7×10^3 CFU/mL) have been observed [49]. It was also
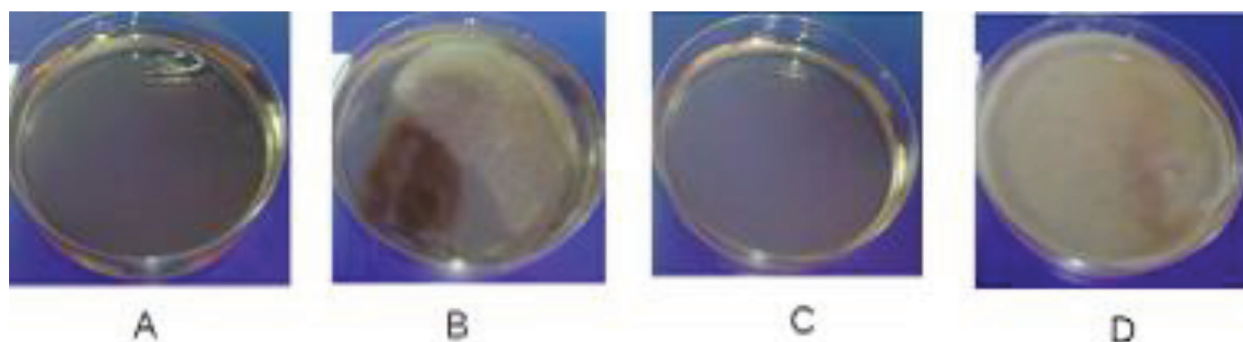
Figure 15. *Kombucha* culture after 7 min irradiation: (A) in the presence of quartz granules, a biofilm on the surface of the liquid is not observable; (B) mat becomes visible when using glass spheres; (C) without metamaterials in the core tube, the mat becomes also visible; (D) the control sample.

revealed that heat treatment is an efficient method to annihilate microorganisms from *Kombucha* tea. For this reason, during experiments, the liquid temperature was preserved below 40°C. Therefore, a thermal inactivation of *Kombucha* microorganisms was ruled out. When *Kombucha* tea is kept at temperatures higher than 20°C, the fungal microbes contribute to biofilm formation (mat). The mat can be therefore inhibited during the storage period by inactivation or removal of the microbes in *Kombucha* tea. The prevention of mat formation is an indication of microorganisms' inactivation during UV-C irradiation. Mat formation was analyzed after 4 days of storage at room temperature. The changes in the rate of microorganisms' inactivation on the metamaterial type were also studied. A more efficient microorganism inactivation was observed for shorter irradiation times when using quartz granules, than in case of irradiation without metamaterials or using glass spheres.

Kombucha culture was inactivated after 7 min irradiation using quartz metamaterials, while mat formation contracted, in direct relation with the irradiation dose. When using quartz granules, the microorganism inactivation is amplified than in the case of glass spheres. After 7 min irradiation in the presence of quartz granules (**Figure 15A**), a mat on the surface of the liquid is not observable. It becomes visible when using glass spheres (**Figure 15B**) or when no metamaterials are present in the core tube (**Figure 15C**). The control sample is presented in **Figure 15D**.

7. Conclusions

A method of annihilation of pathogens using optical metamaterials consisting of microspheres and fiber optical structures having various geometries is suggested. It is proved that using optical metamaterials, like photonic crystal, we get a substantial gain in the decontamination contact surface during the propagation of the contaminated translucent liquid (by viruses and bacteria) through the space between the microspheres (or optical fibers) of metamaterials. The increase of the surface contact of the UV radiation with contaminated liquid strongly depends on the refractive index of metamaterial, liquid volume, and optical properties of viruses and bacteria. We investigated the possibility to trap the viruses and bacteria using an efficient UV decontamination method.

The advancement of nonlinear models based on UV-C interaction with microorganisms opens novel possibilities for the decontamination and diagnosis of different collective processes, which can occur in viruses, bacteria, or other cellular structures under the action of external UV pulses. The possibility to select the UV radiation, which acts on microorganisms with minimal effects, was studied and presented herewith.

The efficient antimicrobial action of the evanescent wave acting around quartz granules in a circulating contaminated translucent liquid when submitted to UV-C irradiation was demonstrated. The treated liquids were polluted water from a natural source, yeast solution, or *Kombucha* fermented tea, while the radiation was generated by 6 UV-C 30 W lamps. Glass microspheres of 1–3 mm diameter were used in experiments, in comparison with quartz unordered granules.

1. Dynamic treatment regime: The complete annihilation of *E. coli* and *Enterococcus* bacteria was observed after 5 min of irradiation; the total elimination of *Coliform* bacteria was achieved after 10 min of irradiation.

   The fermentation of the liquid containing yeast fungi was completely stopped after 15 min UV-C irradiation in the presence of quartz granules. To the contrary, normal fermentation continues after 20 min of irradiation in the absence of optical metamaterials—the case that corresponds to the traditional decontamination method.

2. Static treatment regime: *E. coli* bacteria were completely inactivated in the presence of quartz granules after 1 min irradiation, while in the absence of the quartz metamaterials, some colonies were still present inside the analyzed liquid. This convincingly demonstrates the key role of the quartz metamaterial in fluid decontamination under UV-C irradiation.

   Kombucha-fermented tea microorganisms were completely inactivated after 7 min of treatment using quartz unordered metamaterials. After 7 min of treatment in the presence of glass metamaterials, a thin biofilm may still be observed on the sample surface. Therefore, when using quartz granules, the microorganism inactivation is considerably augmented than in the case of using glass spheres. The biofilm formation on the surface of the liquid after 7 min of treatment becomes visible when using glass spheres, or without metamaterials in the core tube. Mat formation contracted in direct relation with irradiation dose.

   One expects a large increase of the observed effects when passing from simple lamps to laser irradiation, that is, from incoherent to coherent light sources. Also, a significant improvement is expected when using optical fibers for evanescent wave generation instead, or in tandem with, quartz granules.

   Our results prove that the energy emerging via evanescent waves from multistructures submitted to dynamic irradiation is not in any case lost but efficiently used for antimicrobial action. This can contribute to a positive balance of light propagation through PC and PCF metamaterials in view of using light sources with maximum efficiency.

Acknowledgements

Author details

Nicolae Enaki[1], Sergiu Bizgan[1], Andrei Nistreanu[1], Viorica Tonu[1,2], Marina Turcan[1], Tatiana Pislari[1], Elena Starodub[1], Aurelia Profir[1], Gianina-Florentina Popescu-Pelin[3], Maria Badiceanu[3,4], Carmen-Georgeta Ristoscu[3] and Ion N. Mihailescu[3]*

*Address all correspondence to: ion.mihailescu@inflpr.ro

1 Quantum Optics and Kinetic Processes Lab, Institute of Applied Physics, Academy of Sciences of Moldova, Chisinau, Republic of Moldova

2 Department of Human Physiology and Biophysics, State University of Medicine and Pharmacy "Nicolae Testemitanu", Chisinau, Moldova

3 "Laser-Surface-Plasma Interactions" Laboratory, National Institute for Lasers, Plasma and Radiation Physics (INFLPR), Magurele, Ilfov, Romania

4 Physics Department, University of Bucharest, Magurele, Ilfov, Romania

References

[1] Zheludev NI, Kivshar YS. From metamaterials to metadevices. Nature Materials. 2012;**11**: 917-924

[2] Iovine R, La Spada L, Vegni L. Nanoparticle device for biomedical and optoelectronics applications. COMPEL. 2013;**32**(5):1596-1608

[3] Liberal I, Engheta N. Near-zero refractive index photonics. Nature Photonics. 2017;**11**:149-158

[4] Bazgan S, Ristoscu C, Negut I, Hapenciuc C, Turcan M, Ciobanu N, et al. Propagation of UV radiation through meta-materials and its application in bio decontamination. Romanian Reports in Physics. 2015;**67**(4):1602-1607

[5] Enaki N, Profir A, Bazgan S, Paslari T, Ristoscu C, Mihailescu CN, et al. Metamaterials for antimicrobial biofilm applications: Photon-crystals of microspheres and fiber optics for decontamination of liquids and gases. In: Tiwari A, editor. Handbook of Anti-Microbial Coatings. Amsterdam NL, Oxford UK, Cambridge MA USA: Elsevier Inc; 2018. pp. 257-282

[6] Enaki NA, Bazgan S, Ciobanu N, Turcan M, Paslari T, Ristoscu C, et al. Improvement in ultraviolet based decontamination rate using meta-materials. Applied Surface Science. 2017;**417**:40-47

[7] Ashkin A, Dziedzic JM. Optical trapping and manipulation of viruses and bacteria. Science. 1987;**235**(4795):1517-1520

[8] Morrissey MJ, Deasy K, Wu Y, Chakrabarti S, Nic Chormaic S. Tapered optical fibres as tools for probing magneto-optical trap characteristics. Review of Scientific Instruments. 2009;**80**(5):053102

[9] Rowan NJ, MacGregor SJ, Anderson JG, Fouracre RA, McIlvaney L, Farish O. Pulsed-light inactivation of food-related microorganisms. Applied and Environmental Microbiology. 1999;**65**(3):1312-1315

[10] Rosenheck K, Doty P. The far ultraviolet absorption spectra of polypeptide and protein solutions and their dependence on conformation. Proceedings of the National Academy of Sciences. 1961;**47**(11):1775-1785

[11] Sutherland JC, Griffin KP. Absorption spectrum of DNA for wavelengths greater than 300 nm. Radiation Research. 1981;**86**(3):399-410

[12] Tsen KT, Tsen SW, Wu TC, Kibler K, Jacobs B. Selective destruction of viruses with ultrashort pulsed lasers. SPIE Newsroom. 2009:3. DOI: 10.1117/2.1200911.1845

[13] Tsen SW, Wu TC, Kiang JG, Tsen KT. Prospects for a novel ultrashort pulsed laser technology for pathogen inactivation. Journal of Biomedical Science. 2012;**19**(1):62

[14] Zhang C, Li J, Lan L, Cheng JX. Quantification of lipid metabolism in living cells through the dynamics of lipid droplets measured by stimulated Raman scattering imaging. Analytical Chemistry. 2017;**89**(8):4502-4507

[15] Palonpon AF, Ando J, Yamakoshi H, Dodo K, Sodeoka M, Kawata S, et al. Raman and SERS microscopy for molecular imaging of live cells. Nature Protocols. 2013;**8**(4):677

[16] Yamakoshi H, Dodo K, Okada M, Ando J, Palonpon A, Fujita K, et al. Imaging of EdU, an alkyne-tagged cell proliferation probe, by Raman microscopy. Journal of the American Chemical Society. 2011;**133**(16):6102-6105

[17] Kowalski W. UVGI disinfection theory. In: Kowalski W, editor. Ultraviolet Germicidal Irradiation Handbook. Berlin, Heidelberg: Springer; 2009. pp. 17-50. DOI: 10.1007/978-3-642-01999-9_2

[18] Rastogi RP, Kumar A, Tyagi MB, Sinha RP. Molecular mechanisms of ultraviolet radiation-induced DNA damage and repair. Journal of Nucleic Acids. 2010;**2010**:592980. DOI: 10.4061/2010/592980

[19] Schreier WJ, Schrader TE, Koller FO, Gilch P, Crespo-Hernández CE, Swaminathan VN, et al. Thymine dimerization in DNA is an ultrafast photoreaction. Science. 2007;**315**(5812):625-629

[20] Buonanno M, Ponnaiya B, Welch D, Stanislauskas M, Randers-Pehrson G, Smilenov L, et al. Germicidal efficacy and mammalian skin safety of 222-nm UV light. Radiation Research. 2017;**187**(4):493-501

[21] Stein BE, Rahmsdorf HJ, Steffen AN, Litfin MA, Herrlich PE. UV-induced DNA damage is an intermediate step in UV-induced expression of human immunodeficiency virus type 1, collagenase, c-fos, and metallothionein. Molecular and Cellular Biology. 1989;**9**(11):5169-5181

[22] Bhattacharjee C, Sharan RN. UV-C radiation induced conformational relaxation of pMTa4 DNA in *Escherichia coli* may be the cause of single strand breaks. International Journal of Radiation Biology. 2005;**81**(12):919-927

[23] Rothman RH, Setlow RB. An action spectrum for cell killing and pyrimidine dimer formation in Chinese hamster v-79 cells. Photochemistry and Photobiology. 1979;**29**(1):57-61

[24] Sarasin AR, Hanawalt PC. Replication of ultraviolet-irradiated simian virus 40 in monkey kidney cells. Journal of Molecular Biology. 1980;**138**(2):299-319

[25] Miller RL, Plagemann PG. Effect of ultraviolet light on mengovirus: Formation of uracil dimers, instability and degradation of capsid, and covalent linkage of protein to viral RNA. Journal of Virology. 1974;**13**(3):729-739

[26] Smirnov YA, Kapitulez SP, Kaverin NV. Effects of UV-irradiation upon Venezuelan equine encephalomyelitis virus. Virus Research. 1992;**22**(2):151-158

[27] Begley RF, Harvey AB, Byer RL. Coherent anti-Stokes Raman spectroscopy. Applied Physics Letters. 1974;**25**(7):387-390

[28] Bloembergen N. Nonlinear optics. Singapore, New Jersey, London, Hong Kong: World Scientific; 1996. 188 p. DOI: 10.1142/3046

[29] Yan YX, Gamble EB Jr, Nelson KA. Impulsive stimulated scattering: General importance in femtosecond laser pulse interactions with matter, and spectroscopic applications. The Journal of Chemical Physics. 1985;**83**(11):5391-5399

[30] Mannige RV, Brooks CL III. Periodic table of virus capsids: Implications for natural selection and design. PLoS One. 2010;**5**(3):e9423

[31] Zhu T, Ertekin E. Phonon transport on two-dimensional graphene/boron nitride superlattices. Physical Review B. 2014;**90**(19):195209

[32] Zhu T, Ertekin E. Resolving anomalous strain effects on two-dimensional phonon flows: The cases of graphene, boron nitride, and planar superlattices. Physical Review B. 2015; **91**(20):205429

[33] Gilmore R. Catastrophe Theory for Scientists and Engineers. New York: Courier Corporation, Dover Publications Inc; 1993. 666 p

[34] Loudon R. The Quantum Theory of Light. Oxford UK: Oxford University Press; 2000. 448 p

[35] Enaki NA. Non-linear Cooperative Effects in Open Quantum Systems. NY: Nova Science Publishers; 2015. 355 p

[36] Schubert M, Wilhelmi B. Nonlinear Optics and Quantum Electronics. New York: Wiley-Interscience; 1986. 744 p

[37] Enaki N, Colun S. Nonlinear effects in the theory of superconductivity. Journal of Physics: Conference Series. 2012;**338**:012006

[38] La Spada L, Iovine R, Tarparelli R, Vegni L. Conical nanoparticles for blood disease detection. Advances in Nanoparticles. 2013;**2**(3):259-265

[39] Liu Y, Hao Y, Li K, Gong S. Radar cross section reduction of a microstrip antenna based on polarization conversion metamaterial. IEEE Antennas and Wireless Propagation Letters. 2016;**15**:80-83

[40] Iovine R, La Spada L, Vegni L. Nanoplasmonic sensor for chemical measurements. Proceedings of SPIE (Optical Sensors 2013). 2013;**8774**:877411

[41] Cai W, Chettiar UK, Kildishev AV, Shalaev VM. Optical cloaking with metamaterials. Nature Photonics. 2007;**1**:224-227

[42] La Spada L, Bilotti F, Vegni L. Metamaterial resonator arrays for organic and inorganic compound sensing. Proceedings of SPIE (Photonics, Devices, and Systems V). 2011;**8306**: 83060I

[43] Lee Y, Kim S-J, Park H, Lee B. Metamaterials and metasurfaces for sensor applications. Sensors. 2017;**17**:1726

[44] Gusachenko I, Truong VG, Frawley MC, Nic Chormaic S. Optical nano-fibre integrated into optical tweezers for in situ fibre probing and optical binding studies. Photonics. 2015; **2**(3):795-807

[45] Legras JL, Merdinoglu D, Cornuet JM, Karst F. Bread, beer and wine: *Saccharomyces cerevisiae* diversity reflects human history. Molecular Ecology. 2007;**16**(10):2091-2102

[46] Jayabalan R, Malbaša RV, Lončar ES, Vitas JS, Sathishkumar M. A review on kombucha tea—Microbiology, composition, fermentation, beneficial effects, toxicity, and tea fungus. Comprehensive Reviews in Food Science and Food Safety. 2014;**13**(4):538-550

[47] Jonas R, Farah LF. Production and application of microbial cellulose. Polymer Degradation and Stability. 1998;**59**(1–3):101-106

[48] Blanc PJ. Characterization of the tea fungus metabolites. Biotechnology Letters. 1996;**18**(2): 139-142

[49] Jayabalan R, Marimuthu S, Thangaraj P, Sathishkumar M, Binupriya AR, Swaminathan K, et al. Preservation of Kombucha tea effect of temperature on tea components and free radical scavenging properties. Journal of Agricultural and Food Chemistry. 2008;**56**(19): 9064-9071